IEEE Access
Multidisciplinary | Rapid Review | Open Access Journal

Received July 19, 2019, accepted August 12, 2019, date of publication August 30, 2019, date of current version September 27, 2019.

Digital Object Identifier 10.1109/ACCESS.2019.2938549

Design of Spectrum Usage Detection in Wideband Spectrum Measurements

KENTA UMEBAYASHI[1], (Member, IEEE), YOSHITAKA TAMAKI[2], MIGUEL LÓPEZ-BENÍTEZ[3,4], (Senior Member, IEEE), AND JANNE J. LEHTOMÄKI[5], (Member, IEEE)

[1]Department of Electrical and Electronic Engineering, Tokyo University of Agriculture and Technology, Tokyo 183-8538, Japan
[2]TAIKI-SHA Ltd., Yokohama, 225-0003, Japan
[3]Department of Electrical Engineering and Electronics, University of Liverpool, Liverpool L69 3GJ, U.K.
[4]ARIES Research Centre, Antonio de Nebrija University, 28040 Madrid, Spain
[5]Centre for Wireless Communications (CWC), University of Oulu, 90570 Oulu, Finland

Corresponding author: Kenta Umebayashi (ume_k@cc.tuat.ac.jp)

This work of K. Umebayashi was supported in part by the European Commission in the Framework of the H2020-EUJ-02-2018 Project 5G-Enhance under Grant 815056, in part by the Ministry of Internal Affairs and Communications (MIC) of Japan, in part by the JSPS KAKENHI under Grant JP18K04124 and Grant JP18KK0109, and in part by the Institute of Global Innovation Research in TUAT. The work of M. López-Benítez was supported by the British Council through the UKIERI DST Thematic Partnerships 2016–2017 under Grant DST-198/2017. The work of J. J. Lehtomäki was supported in part by Infotech Oulu, and in part by the Academy of Finland 6Genesis Flagship under Grant 318927.

ABSTRACT We investigate the design of signal processing in wideband spectrum usage (SPU) measurements for efficient and smart dynamic spectrum access (DSA). In particular, we focus on spectrum usage detection (SPUD) in the experimental measurements. The detection results can be exploited to estimate statistics of the SPU. An appropriate design of the SPUD depends on the actual SPU in the target frequency band. There is a broad range of wireless systems in a considered broad measurement frequency band, such as from 60MHz to 6GHz, therefore a general design framework in the measurement frequency band is desired. In the proposed design framework, we at first define two models in terms of the SPU and the SPUD process. In addition, the proposed design procedure determines the adequate choice of parameters for the SPUD model based on given parameters of the SPU model in the target frequency band. Numerical evaluation based on computer simulations shows the validity of the design framework and design procedure. Moreover, a modified duty cycle (DC) estimation method is proposed, which can remove bias errors caused by low time resolution in the SPUD. Numerical evaluation based on experimental measurements demonstrates the practicality of the detection framework and procedure proposed in this work.

INDEX TERMS Dynamic spectrum access, smart spectrum access, SPU measurement, duty cycle estimation, overlap FFT, energy detection.

I. INTRODUCTION

In the wireless communication field, spectrum scarcity is an urgent issue. Since most of the spectrum has been exclusively assigned to licensed wireless systems, there are not enough spectrum resources for new emerging wireless services. On the other hand, spectrum utilization measurement reports have revealed that the utilization rate of most of the licensed spectrum is not very high in spatial and/or temporal domains [1]. One possible solution for this issue is *spectrum sharing* since it can make the underutilized spectrum resource available to the emerging wireless services [2], [3]. In fact, several types of spectrum sharing approaches have been investigated, such as dynamic spectrum access (DSA) [4], [5], licensed shared access (LSA) [6], and spectrum access system with citizens broadband radio service (CBRS) [7], with different types of priorities and licensing.

In DSA, a secondary user (SU) can utilize spectrum licensed to a primary user (PU), as long as the spectrum usage (SPU) by SU does not cause any harmful interference towards the PU [4], [5]. There are two important key techniques: spectrum sensing and spectrum management. The spectrum sensing can detect instantaneous status of spectrum and SU can find vacant spectrum. The spectrum management includes spectrum allocation and channel selection to utilize the vacant spectrum efficiently. These key techniques

The associate editor coordinating the review of this manuscript and approving it for publication was Faisal Tariq.

can be designed properly based on PU SPU, which can be characterized by appropriate SPU statistics [8]. For example, the knowledge of the duty cycle (DC) can enhance spectrum sensing performance [9]–[11], spectrum management [12]–[15] and channel selection [16].

In [17], the concept of smart spectrum access (SSA), which is an enhanced form of DSA, has been presented. In SSA, the prior information of PU SPU is exploited to enable an enhanced DSA. Two-layered SSA has been proposed as a practical implementation of SSA as shown in Fig. 1. This two-layered SSA concept consists of DSA as the first layer and a spectrum awareness system (SAS) as the second layer. SAS is dedicated for SPU measurements to extract useful PU activity information so that SUs in DSA can be relieved of having to perform energy and time consuming SPU measurements. The SPU information, based on long term, wide band, and broad area spectrum measurements, is stored in a data base. The long term information is processed by adequate SPU modeling to extract a set of parameters sufficiently characterizing the full information (which would be impractical to share) [18]. In this paper, we focus on the spectrum measurement which is used to estimate statistical information of SPU based on long term measurements. This is different from the spectrum sensing which attempts to obtain an instantaneous status of SPU.

There have been many SPU measurement campaigns (see [15], [19]–[22] and references therein). Measurement campaigns have shown the DC and measured power of various spectrum bands at various measurement sites [23]–[27]. This type of measurement campaigns has simply evaluated spectrum utilization and potential spectrum opportunities (i.e., how much spectrum in a certain dimension, such as time and space, is vacant). In [8], estimation of SPU statistics based on periodic SPUD is investigated. This investigation reveals that the measurement process imposes on accuracy of the estimation. There are also detailed SPU models in time, frequency and space domains, respectively [28]–[31]. In these investigations, not only the spectrum utilization ratio, but also the trends and variations of feature quantities of spectrum utilization, such as DC [28], signal strength [30] and busy time (vacant time) [16], [32], have been considered. A probabilistic storage algorithm is also investigated to store a measurement data [33]. The proposed algorithm can reduce the storage volume for the spectrum measurement results by approximately 99%.

In most SPU measurements, energy detection (ED) has been employed for SPUD in the time-frequency domain. In ED, averaging the observed power spectrum in the time and frequency domains is typically employed to enhance the detection performance. This area for averaging is referred to as *mask* in this paper. The mask size affects the detection performance as well as the time and frequency domain resolutions. This implies that the applicable parameters for SPUD and statistics estimation strongly depend on the characteristics of the PU SPU itself. In broadband measurements covering a variety of wireless systems, the SPUD has to be designed by taking into account the heterogeneous features of the systems present in the considered frequency span. However, to the best of the authors' knowledge, this approach has not been deeply investigated.

In this paper, we investigate the design of a SPU measurement by considering the characteristics of the PU SPU. Specifically, we focus on SPUD and the following DC statistics estimation. In SPUD, ED with overlapping fast Fourier transform (FFT), such as Welch FFT, is typically employed [34], [35]. Our main contributions are summarized as follows:

- A design framework for SPU measurements is proposed. The proposed framework consists of three items: a model of SPU, a model of SPUD, and a design procedure to set adequate parameters for SPUD based on the parameters of the SPU model. This framework has broad utility, which is a desirable aspect for the broadband SPU measurement in SAS.
- For the SPUD, the detection performance in terms of detection probability and false alarm probability is used as design criterion. Analysis of the detection performance including effects of correlation in the time samples is derived. This strict analysis enables an optimum parameter setting for SPUD.
- The above mentioned analysis may require a large number of significant figures, which may increase the computation time significantly. To address this issue, a deflection coefficient based analysis is also shown. Numerical results will show that design procedure based on the deflection coefficient can reduce complexity of the parameter setting procedure.
- In a typical DC estimation, a high frequency/time resolution in the SPUD leads to relatively low detection performance due to the lack averaging (corresponding to low time bandwidth product) and it deteriorates the DC estimation under low signal to noise power ratio (SNR). On the other hand, low resolution leads to significantly biased/erroneous DC estimation under high SNR. To address this issue, we propose a modified DC estimation method to remove the biased estimation error in the region of high SNR.
- The validity of the proposed design (framework and procedure) and the modified DC estimation are confirmed by computer simulations, and spectrum measurement campaigns in various SPU scenarios (LTE: long term evolution, DECT: digital enhanced cordless telecommunications, and SCPC/FDMA: single channel per carrier/frequency division multiple access).

The remainder of this paper is organized as follows. First, Section II summarizes the considered design framework including the models of SPU and assumed SPUD processing. Section III presents the proposed design procedure for SPUD. Specifically, the design criterion and design procedure to determine the model parameters for the SPUD are shown. In Section IV, a modified DC estimation based on the SPUD results is proposed. In Section V, numerical evaluations based

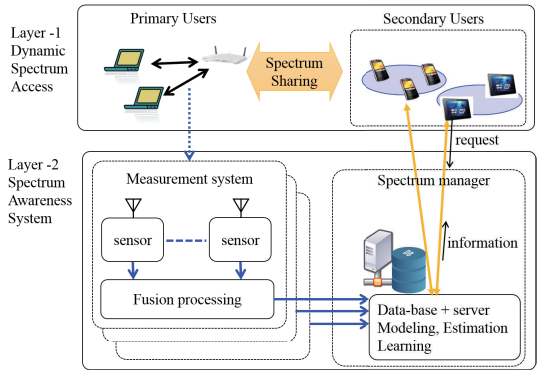

FIGURE 1. Concept of two-layered smart spectrum access (SSA).

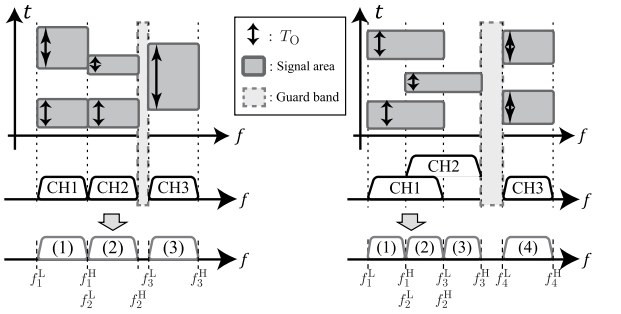

(a) Non-overlapping channel allocation (b) Overlapping channel allocation

FIGURE 2. Two types of channel allocation and example of channel usage in the time-frequency domain.

on computer simulations and three SPU measurement campaigns are provided to verify the validity of the proposed design and DC estimation. Finally, Section VI concludes this paper.

II. DESIGN FRAMEWORK

We consider SPU measurement based on the two-layered SSA concept, shown in Fig. 1. The spectrum measurement system in SAS consists of several sensors and one fusion center. The main role of the measurement system is to observe the SPU of PUs and to send measurement reports to a database server in the SAS. The measurement systems are deployed in the space domain to observe wide bandwidths (such as from 60MHz to 6GHz) for long time (such as a few dozen days). In this paper, we employ real-time spectrum analyzer Tektronix RSA 6100A as a sensor [18] which can observe large instantaneous bandwidths up to 110 MHz without any time domain gaps between the outputs. Therefore, within the instantaneous bandwidth real-time spectrum analyzer leads to much more accurate results. Most of the measurements to date have used conventional swept spectrum analyzers that can miss signals that occur between the sweeps. For wide-band (several GHz) measurements real time spectrum analyzer utilizing frequency stepping still leads to more accurate results as during the dwell time (which should be set large enough) on each sub-band there are no time domain gaps. In the measurement system, each sensor sends the local measurement information (such as DC estimation) to the fusion center. The fusion center integrates the reported measurement information and sends the integrated information to the database server in SAS. In this paper, we focus on the signal processing for SPU measurement in particular, SPUD, at the sensor. The results of SPUD are used to understand the characteristics of SPU and we investigate a DC estimation method. The measurement frequency bandwidth covers a large variety of wireless systems and the SPUs of these wireless systems are heterogeneous.

In the proposed design framework, we define a model of SPU and a model of SPUD. Each model consists of different model parameters. The parameters for the SPU model capture the characteristics of the PU's SPU and are determined by the specification of the corresponding wireless system. Based on such model parameters, the reasonable parameters for the SPUD can be determined with the proposed design procedure. In the following, both models are presented.

A. MODEL OF SPU

Under extremely wide measurement bandwidths, it is difficult to observe the whole bandwidth simultaneously due to the limited capabilities of sensors. Therefore, the whole frequency band is divided into sub-measurement bands. We consider several sub-measurement bands W_i where i ($i = \{1, 2, \cdots, I\}$) is the index number of the sub-measurement band. The partitioning rule for the sub-measurement bands is based on the wireless service and system as well as the capability of the sensor. Specifically, in a sub-measurement band, there may be a target wireless system or several wireless systems sharing the frequency band. This partitioning rule is very natural since the SPU parameters can be determined by the wireless system. The adequate parameters of SPUD are determined for the target wireless system in each sub-measurement band. In the numerical evaluations, specific sub-measurement bands, such as LTE-uplink, are considered in Sect. V-C, otherwise a general wireless system is assumed in this paper.

Now we focus on one sub-measurement band with a general wireless system. Typically, there are several channels in the sub-measurement band. Two types of channel configuration are assumed: a non-overlapping channel allocation and an overlapping channel configuration. Examples of both types of channel configuration and channel usage are shown in Fig. 2. The signal area indicates an area occupied by one signal component, such as one data packet, in the time and frequency domain. The channel configuration characterizes the SPU in the frequency domain by the model as shown in Fig. 2, which can be expressed in matrix form as

$$\mathbf{F}_{CH} = \begin{bmatrix} f_1^L & f_2^L & f_3^L & \cdots & f_{I_f}^L \\ f_1^H & f_2^H & f_3^H & \cdots & f_{I_f}^H \end{bmatrix}. \quad (1)$$

where two edges are used in the frequency domain in each channel. Frequency bands $[f_l^L \ f_l^H]^t$, where $[\cdot]^t$ indicates

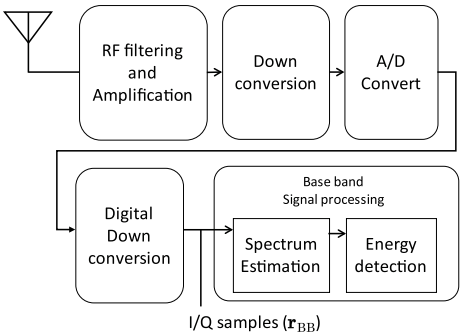

FIGURE 3. Block diagram of process in a sensor.

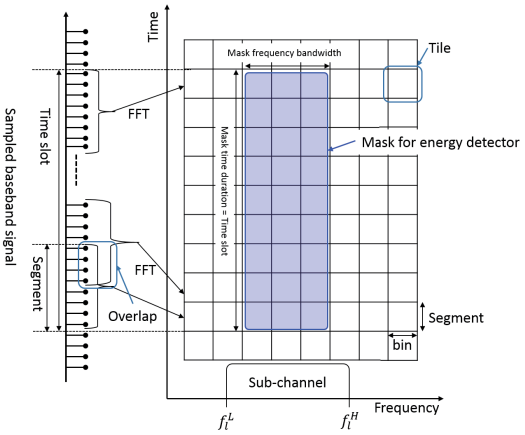

FIGURE 4. Mask for ED and FFT process with an overlapping.

transposition for a matrix/vector, corresponds to a minimum unit of SPU in the frequency domain and this is denoted by the lth *sub-channel*. As it can be seen from Fig. 2(b), the division to sub-channels is such that within each sub-channel there is a constant number of systems present. Therefore, the sub-channels that we discuss here can be smaller than the channels used by the PUs. Frequency bands not occupied by signal components, such as guard bands, are not included in $\mathbf{F}_{CH}$. In the SPU measurement, statistics of SPU, such as the DC, in the frequency sub-channel l between f_l^L and f_l^H are estimated.

In the time domain, we use the time duration for one continuous spectrum occupation period as a model parameter. The time duration is denoted by T_O. This time duration may be time-variant and we use its minimum value, $T_{O,\min} = \min\{T_O\}$, to characterize the PU SPU in time domain. In particular, $T_{O,\min}$ is used to determine the required time resolution for the SPUD. At the lth sub-channel, the minimum signal area is defined by the minimum time-duration $T_{O,\min}$ and the frequency band $f_l^H - f_l^L$, respectively.

B. MODEL OF SPUD

An outline of the signal processing in each individual sensor is shown in Fig. 3. The received signal is down-converted to baseband signal through the RF (Radio Frequency) and IF (Intermediate Frequency) processing in the sensor. We consider the following model of baseband signal processing in the sensor. An input vector $\mathbf{r}_{BB} = [r_{BB,1}, \ldots, r_{BB,N_{ob}}]^t$ represents the observed complex base-band signal where N_{ob} is the number of samples. The measurement frequency band is set to $[f_c - f_s/2, f_c + f_s/2]$ where f_s denotes sampling rate, and f_c is the center frequency for the sub-measurement band.

For the SPUD, we employ ED implemented with overlapping FFT. The threshold for ED is set based on the Constant False Alarm Rate (CFAR) criterion [36]. In the assumed overlapping FFT, power spectrum is obtained by averaging multiple estimations based on overlapping FFTs [37]. The number of samples for one FFT and one Welch FFT using overlapping individual FFTs are denoted by N_{FFT} and N_{time} ($N_{time} > N_{FFT}$), respectively, where N_{FFT} is a power of two. The time duration for one overlapping FFT is considered equal to the duration of one time slot. Specifically, N_{time} samples in a time slot are divided into multiple segments with N_{FFT} samples per segment. In the neighboring segments, a part of samples overlap with an overlap ratio equal to $\gamma = 0.5$ [37]. The relationship among the number of segments in N_{time}, N_{FFT}, and γ is given by

$$N_{seg} = \frac{N_{time} - N_{FFT}}{N_{FFT}(1-\gamma)} + 1 = \frac{2N_{time}}{N_{FFT}} - 1. \tag{2}$$

In the kth segment, the samples for one FFT is given by

$$\mathbf{r}_k = [r_{k(\gamma N_{FFT})+1}\ r_{k(\gamma N_{FFT})+2}\ \cdots\ r_{k(\gamma N_{FFT})+N_{FFT}}]^T. \tag{3}$$

The FFT result for $\mathbf{r}_k$ is

$$\mathbf{x}_k = \mathbf{F}\mathbf{W}\mathbf{r}_k \tag{4}$$

where diagonal matrix $\mathbf{W}$ represents a window function, such as the Hamming window, and $\mathbf{F}$ is a discrete Fourier transform matrix given by

$$\mathbf{F} = \begin{bmatrix} \alpha^0 & \alpha^0 & \cdots & \alpha^0 \\ \alpha^0 & \alpha^1 & \cdots & \alpha^{N_{seg}-1} \\ \vdots & \vdots & \ddots & \vdots \\ \alpha^0 & \alpha^{N_{seg}-1} & \cdots & \alpha^{(N_{seg}-1)(N_{seg}-1)} \end{bmatrix}, \tag{5}$$

where $\alpha = \exp(2\pi j/N_{FFT})$. The estimated power spectrum at the kth segment and the bth frequency bin is given by $P_s(k,b) = x_{k,b}x_{k,b}^*$ where $*$ indicates complex conjugation and $x_{k,b}$ is the bth sample in the vector $\mathbf{x}_k$.

Let us define a tile as a single element of the grid corresponding to one time slot and one frequency bin. The role of SPUD is to recognize the state of each tile: either occupied by a signal component or not. In a typical SPU measurement, the signal occupancy state in each tile corresponding to one frequency bin b and one segment k is detected. On the other hand, we employ mask-based ED and design a mask for ED based on the SPU model parameters $T_{O,\min}$ and $\mathbf{F}_{CH}$. Fig. 4 shows the mask and FFT process in one time slot. The mask indicates the area over which the observed power spectrum in the tiles is averaged. The averaged energy is used as a decision variable in ED. The mask is designed for each sub-channel

as shown for the lth sub-channel in Fig. 4. The shape of the mask is a rectangle and has two components, namely the mask frequency bandwidth and mask time duration [38]. These two components are expressed by the number of bins and the number of segments, respectively. The mask time duration is equal to the time slot length N_{time}. For the lth sub-channel $[f_l^L\ f_l^H]^t$, the mask frequency bandwidth is determined by a region of frequency bins between b_l^L and b_l^H, where b_l^L and b_l^H are the lower and the upper limits of frequency bins for the lth mask frequency bandwidth, respectively. This means that the frequency bins in the mask bandwidth are fully occupied by signals when signal is present. The matrix of the mask frequency bandwidth for all sub-channels is defined by

$$\mathbf{B}_{CH} = \begin{bmatrix} b_1^L & b_2^L & b_3^L & \dots & b_{l_{end}}^L \\ b_1^H & b_2^H & b_3^H & \dots & b_{l_{end}}^H \end{bmatrix}, \tag{6}$$

where l_{end} indicates the number of sub-channels.

The ED principle is employed in each mask and the test statistic T_{ED} is given by

$$T_{ED} = \frac{1}{N_{ave}} \sum_{(b,k)\in\mathbf{M}} P_s(k,b) \tag{7}$$

where $\mathbf{M}$ is the set of tiles in the mask and $N_{ave} = |\mathbf{M}|$ is the number of tiles in the mask.

SPUD is represented by a binary hypothesis problem where hypothesis H_0 indicates that there is no signal component in the mask and H_1 indicates that all tiles in the mask are occupied by signal component. The cases, in which the mask is partially occupied by the signal component are not considered. In Section V, we evaluate the effect of partial occupation on the DC estimation. The SPUD rule is given by

$$\hat{H} = H_0 : T_{ED} < \eta$$
$$\hat{H} = H_1 : T_{ED} \geq \eta$$

where $\hat{H}$ is the decision result and η is the threshold for ED. To evaluate the SPUD, we define the detection probability P_D as $P_D = \Pr(\hat{H} = H_1|H_1)$ and false alarm probability P_{FA} as $P_{FA} = \Pr(\hat{H} = H_1|H_0)$. By assuming additive white Gaussian channel noise model, the resulting P_{FA} in the overlapping FFT based ED is given by [39]

$$P_{FA} = \sum_{k=1}^{N_{time}} \frac{\left(\lambda_k^{(H_0)}\right)^{N_{FFT}-1}}{\prod_{1\leq l\leq N_{time},\ l\neq k} (\lambda_k^{(H_0)} - \lambda_l^{(H_0)})} \exp\left(-\frac{N_{time}\eta}{\lambda_k^{(H_0)}}\right) \tag{8}$$

where $\lambda_k^{(H_0)}$ is an eigenvalue of $E\left[\mathbf{x}_{mask,l}\mathbf{x}_{mask,l}^H\right]$ under H_0, $\mathbf{x}_{mask,l}$ is a vector with the elements $x_{k,b}$ in the mask for the lth sub-channel, and $E[\cdot]$ is the expectation operator. According to the CFAR criterion, η is set to satisfy a target false alarm probability $\dot{P}_{FA}$. The decision threshold for a target $\dot{P}_{FA}$ can be obtained by solving (8). For the CFAR criterion, noise floor information is necessary to set the threshold for $\dot{P}_{FA}$. To this end we employ the forward consecutive mean excision (FCME) algorithm for noise floor estimation proposed in [34], [40]. The analytical P_D is given by [39]

$$P_D = \sum_{k=1}^{N_{ave}} \frac{\left(\lambda_k^{(H_1)}\right)^{N_{FFT}-1}}{\prod_{1\leq l\leq N_{ave},\ l\neq k} (\lambda_k^{(H_1)} - \lambda_l^{(H_1)})} \exp\left(-\frac{N_{ave}\eta}{\lambda_k^{(H_1)}}\right), \tag{9}$$

where $\lambda_k^{(H_1)}$ is an eigenvalue of $E\left[\mathbf{x}_{mask,l}\mathbf{x}_{mask,l}^H\right]$ under H_1 and the signal component is assumed to be Gaussian signal. A detailed analytical derivation of the eigenvalues $\lambda_k^{(H_0)}$ and $\lambda_k^{(H_1)}$ is shown in the appendix.

For an adequate SPUD, N_{FFT} and the mask size, i.e., the time slot size N_{time} and mask frequency bandwidth matrix $\mathbf{B}_{CH}$, have to be determined. Therefore, the relevant model parameters of SPUD are N_{FFT}, N_{time} and $\mathbf{B}_{CH}$. The design procedure for these parameters is described in Section III.

III. DESIGN PROCEDURE FOR THE SPUD

For the design of the SPUD, we use the detection probability P_D as the main criterion. Specifically, for a given set of parameters, $T_{O,\min}$ and $\mathbf{F}_{CH}$, the proposed design procedure can set the model parameters of SPUD, N_{FFT}, N_{time}, and $\mathbf{B}_{CH}$, to maximize P_D. The parameters of SPUD are mainly related to the mask design. The preferred design approach/principle of a mask is that the mask is inside the signal area and covers the minimum signal area (time length: $T_{O,\min}$ and frequency width: $[f_l^L\ f_l^H]^T$) as much as possible.

We now consider the parameter setting for the lth sub-channel $[f_l^L\ f_l^H]^T$ based on the mentioned design approach. In this case, model parameters of the SPUD are N_{FFT}, N_{time}, and $[b_l^L\ b_l^H]^T$. In the lth sub-channel, the frequency domain SPU is expressed by $[f_l^L\ f_l^H]^T$, which is time invariant. Therefore, an adequate parameter setting $[b_l^L\ b_l^H]^t$ for a specified N_{FFT} is given by

$$b_l^L = \left\lceil \frac{f_l^L - f_c}{f_s/N_{FFT}} + \frac{1}{2} \right\rceil$$
$$b_l^H = \left\lfloor \frac{f_l^H - f_c}{f_s/N_{FFT}} - \frac{1}{2} \right\rfloor \tag{10}$$

where $\lfloor\cdot\rfloor$ is the floor function and $\lceil\cdot\rceil$ is the ceiling function. The selected lth mask frequency bandwidth is set to cover a signal area in the frequency domain as large as possible, provided that it is inside the lth sub-channel $[f_l^L\ f_l^H]^T$. On the other hand, it is difficult to keep the mask inside the signal area in the time domain since the SPU measurement and the observed signal are not synchronized. Therefore, we set a constraint in terms of possible offset error due to the asynchronicity operation as

$$N_{FFT}/f_s \leq R_t T_{O,\min}, \tag{11}$$

where R_t indicates the possible offset error ratio of $T_{O,\min}$, which typically is $R_t < 1$. Specifically, the maximum allowable overestimation error in time length is $R_t T_{O,\min}$ in the edge of the signal area. According to this constraint, the time

duration of time slot has to be less than $R_t T_{O,\min}$. Based on this constraint, N_{time} in the given N_{FFT} can be obtained as

$$N_{time} = N_{FFT}\left\{1+(1-\gamma)\left\lfloor \frac{1}{1-\gamma}\left(\frac{R_t T_{O,\min} f_s}{N_{FFT}}-1\right)\right\rfloor\right\}. \quad (12)$$

Equations (11) and (12) indicate that an adequate value of $[b_l^L\ b_l^H]^t$ and N_{time} depends on N_{FFT}. The optimum FFT size N_{FFT}^{opt} is therefore given by

$$N_{FFT}^{opt} = \arg\max_{N_{FFT}} P_D, \quad (13)$$

subject to the constraint in (11). An exhaustive search is a straight forward approach to show this optimization problem, however the numerical calculation of (9) requires a huge number of significant figures to achieve an accurate calculation. The number of significant figures required for an accurate calculation in (9) is about five hundreds. For comparison the double precision floating point numbers typically used for numerical computations have only about fifteen significant figures. For example, in MATLAB, this means that much more costly variable-precision arithmetic needs to be used.

For the issue of computational cost, we also investigate a simpler approach for the model parameter setting. Instead of P_D, a modified deflection coefficient D is employed to obtain N_{FFT}^{opt}. The modified deflection coefficient is defined as [41]–[43]

$$D = \frac{(E\left[T_{ED}|H_1\right] - E\left[T_{ED}|H_0\right])^2}{var\left[T_{ED}|H_0\right] + var\left[T_{ED}|H_1\right]}, \quad (14)$$

where $var\left[\cdot\right]$ is the variance function. The analytical derivations of $E\left[T_{ED}|H_i\right]$ and $var\left[T_{ED}|H_i\right]$ are shown in the appendix. In the design procedure based on D, we also perform an exhaustive search to find N_{FFT}^{opt}.

We have discussed the optimum parameter setting for an individual sub-channel. In most cases, there may be multiple sub-channels in the measured sub-band. In this case, we need to consider the worst case to set the value of N_{FFT}. Let $D_l(N_{FFT})$ denote the achievable modified deflection coefficient with N_{FFT} in the lth sub-channel. The optimum N_{FFT} for the lth sub-channel in the sub-band is obtained as

$$N_{FFTopt}^{(l)} = \arg\max_{N_{FFT}} \left[D_l(N_{FFT})\right], \quad (15)$$

Then, optimum N_{FFT} for the sub-band is

$$N_{FFT}^{opt} = \arg\min_{N_{FFTopt}^{(l)}} \left[D_l(N_{FFTopt}^{(l)})\right]. \quad (16)$$

In the case of P_D, we can use the same procedure to obtain N_{FFT}^{opt} for the sub-band.

IV. MODIFIED DUTY CYCLE ESTIMATION

In this section, two DC estimation methods are proposed. The first one is conventional DC estimation method used as the reference and the second one is a modified DC estimation method. We consider the estimation of DC in the lth sub-channel, where a detection result in the mth mask in the time domain is denoted by

$$S(m) = 0, \quad \hat{H} = H_0$$
$$S(m) = 1, \quad \hat{H} = H_1,$$

In the reference DC estimation method, the DC Ψ_R is estimated as

$$\Psi_R = \sum_{m=0}^{N_S-1} S(m)/N_S, \quad (17)$$

where N_S denotes the number of decision results. Let $\mathbf{S}$ denote a vector $\mathbf{S} = [S(0), \cdots, S(N_S-1)]^T$. Altered process in the modified DC estimation is explained for $\mathbf{S} = [0100111110]^T$ as follows. The signal area and detection results in the lth sub-channel are shown in Fig. 5. The signal area in this example is the minimum signal area. In Fig. 5, the left-hand side corresponds to $\mathbf{S}$ (before the altered process) and right hand corresponds to the output after the altered process $\bar{\mathbf{S}}$. In this example, $R_t = 1/4$ is assumed, therefore the mask size in the time domain is approximately one quarter of the time length of the minimum signal area.

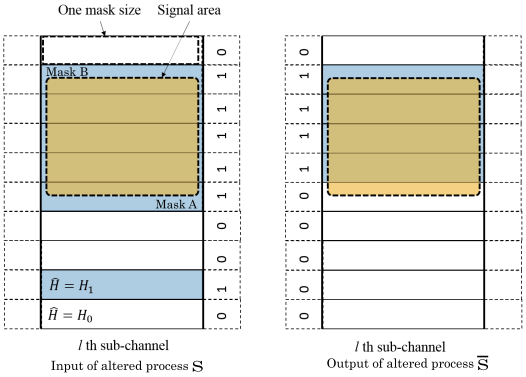

FIGURE 5. Input (left-hand) and output (right-hand) for altered process in the modified DC estimation.

The altered process extracts the clusters of ones (“1”), which in the example of Fig. 5 there are two clusters in $\mathbf{S}$, i.e., “1” and “11111”. In each cluster, the first “1” is changed to “0”, which leads to a output vector $\bar{\mathbf{S}} = [0000011110]^T$. There are two aims in the altered process to achieve an accurate DC estimation. If there is a false alarm error, the cluster size may be one. Specifically, the first “1” in $\mathbf{S}$ may be a false alarm error and the altered process can remove it. Under high SNR case, even the partially occupied masks will lead to detection, $S(m) = 1$ and this leads to overestimation in the DC estimation. This is shown as “Mask A” and “Mask B” in the left hand size in Fig. 5. In this example, correct time length is four mask sizes, but estimated time length by the reference DC estimation is five mask sizes (left hand in Fig. 5). As the altered process correctly outputs length of four mask sizes (’11111’ was changed to 1111), the altered process can suppress the biased error. This is true

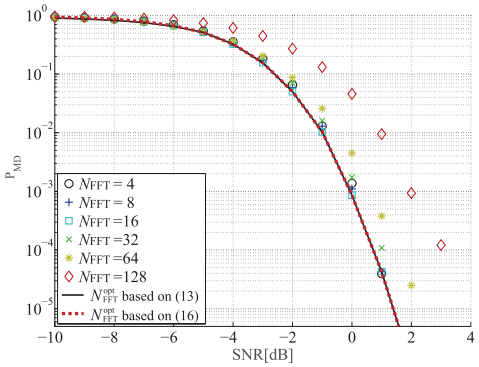

FIGURE 6. P_{MD} performance as a function of SNR with $R_t = 1/4$ and $P_{FA} = 0.01$ for different FFT sizes.

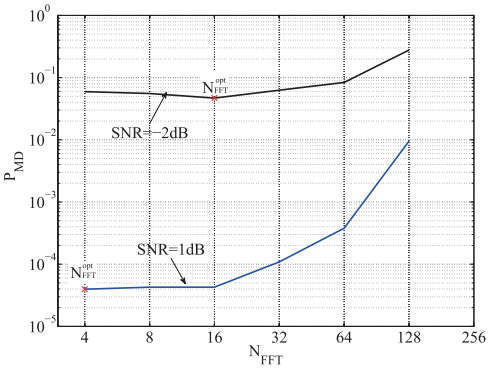

FIGURE 7. P_{MD} performance as a function of SNR with $R_t = 1/4$ and $P_{FA} = 0.01$ for different FFT sizes.

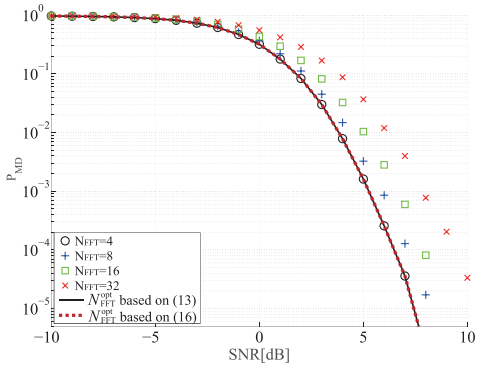

FIGURE 8. P_{MD} performance as a function of SNR with $R_t = 1/16$ and $P_{FA} = 0.01$ for different FFT sizes.

also in general case. The reasoning for this process that if we have sufficient SNR, the two partially occupied masks at the beginning and end (Mask A and Mask B in Fig. 5) will be both classified to be '1', leading to overestimation of length. By removing one '1' in the altered process, we recover the true length.

In the modified DC estimation, the estimated DC Ψ_M is given by

$$\Psi_M = \sum_{m=0}^{N_S-1} \bar{S}(m)/N_S, \tag{18}$$

where $\bar{S}(m)$ is the mth element of $\bar{\mathbf{S}}$.

V. SIMULATION AND EXPERIMENTAL RESULTS

We first evaluate the SPUD based on the proposed design (design framework and design procedure) and the DC estimation performances by means of computer simulations. Afterwards, we also confirm the practical validity of the proposed design based on experimental SPU measurement results in different wireless systems.

In computer simulations, we consider one sub-channel. The bandwidths of the sub-measurement (all bins in Fig. 4) band and sub-channel are 12.5 and 6MHz, respectively. The sampling rate is equal to 12.5 Msamples/s. The minimum time duration $T_{O,\min}$ is set to 50 μsec, which leads to 625 samples in a mask. Since we consider the downconverted signal, the center frequencies for the sub-measurement band and the sub-channel are assumed to be $f_c = 0$ Hz and $f_c^{(l)} = 0$ Hz, respectively, without loss of generality. The assumed signal size is the minimum signal area (i.e. time duration is $T_{O,\min}$) which corresponds to the worst case for DC estimation.

A. COMPUTER SIMULATIONS (DETECTION PERFORMANCE)

We first evaluate the detection performance of SPUD by means of the miss detection probability which is given by $P_{MD} = 1 - P_D$ with a given false alarm probability. In Fig. 6, the P_{MD} performance is shown as a function of SNR for $R_t = 1/4$. There are two types of results: the first one is for fixed FFT size (such as $N_{FFT} = 4, 8, 16, 32, 64, 128$) and the second one uses N_{FFT}^{opt} with the criteria (13) or (16). In the second type, the optimum N_{FFT} depends on the SNR. We can confirm that N_{FFT}^{opt} based SPUD can always achieve the best detection performance for any SNR. Moreover, the achieved detection performances by (13) and (16) criteria are the same. This indicates the validity of the efficient design procedure based on the deflection coefficient D in (16).

To confirm the optimum FFT size, the P_{MD} performance as a function of N_{FFT} is shown in Fig. 7 for the cases of SNR=-2dB ($N_{FFT}^{opt} = 16$) and SNR=1dB ($N_{FFT}^{opt} = 4$), respectively. These results show that N_{FFT}^{opt} depends on the SNR.

In Fig. 8, the P_{MD} performance is shown as a function of SNR with $R_t = 1/16$. Again we can confirm the validity of the proposed design procedures since the P_{MD} performance obtained by the proposed design procedures are the best.

In both Figs. 6 and 8, there is not any significant performance difference between the P_D and D design criteria. An advantage of the D based design procedure is a lower computational cost compared to the P_D based design procedure. The computational time ratio of the design procedure based on D to the design procedure based on P_D is plotted in Fig. 9. In the criterion based on P_D (9), a large number of significant figures, such as 500 digits, is required to avoid

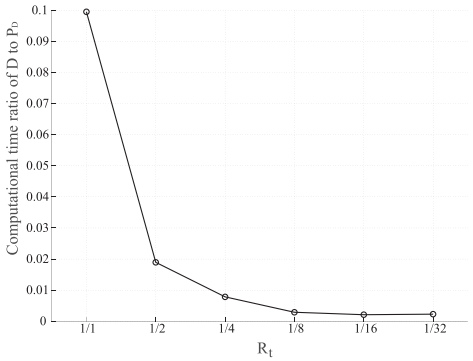

FIGURE 9. Computational time ratio of D to P_D as a function of R_t performance.

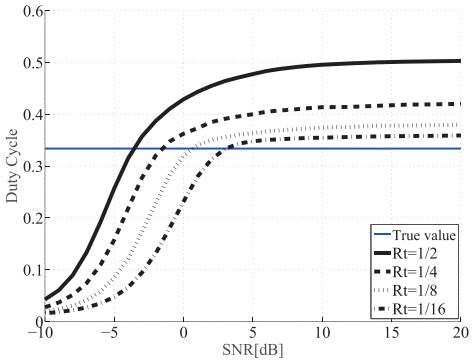

FIGURE 10. Duty Cycle estimation (reference method) as a function of SNR for different R_t, the conventional DC estimation is used.

not a number (NaN) in a calculation of P_D in (9). On the other hand, with the design criterion based on D, double precision floating point numbers are enough. This result indicates that the ratio decreases as R_t is reduced. The computational time of the design procedure based on D is at most 10% of the time of the design procedure based on P_D.

B. COMPUTER SIMULATIONS (DC ESTIMATION PERFORMANCE)

The reference DC estimation method in (17) and the modified DC estimation method in (18) are evaluated in terms of the DC estimation performance in Fig. 10 for different R_t. In the low SNR region (less than -5 dB), large R_t can achieve higher detection performance which leads to accurate DC estimation. Notice that large R_t values lead to a large number of tiles in the mask, which inherently achieves high detection performance. In the high SNR region, large R_t leads to lower time resolution and therefore significantly large bias. For smaller bias the convergent DC estimation, smaller R_t is required, which in turn requires high SNR for an accurate DC estimation.

Fig. 11 shows the DC estimation performance of the modified DC estimation method for different R_t. They can achieve accurate DC estimation performance compared to the reference DC estimation method in high SNR region. Large R_t, such as $R_t = 1/2$, provide a good leading edge in low SNR

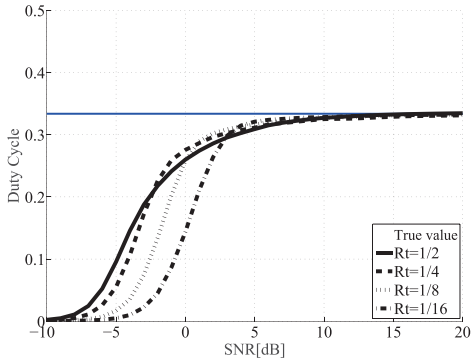

FIGURE 11. Duty Cycle estimation (modified method) as a function of SNR for different R_t, the modified DC estimation is used.

region but a slightly poor convergence to the true value and vice versa. Therefore, $R_t = 1/4$ is an appropriate option in this case. An advantage of the modified DC estimation is that the biased error can be removed in the high SNR region (beyond 10 dB) for any R_t.

With the reference method (Fig. 10) the estimated DC is accurate only if the SNR takes a particular value, otherwise the estimation is in general very inaccurate due to the false alarms due to the overestimation in the DC estimation. On the other hand, the estimation provided by the modified method (Fig. 11) is very accurate over a wide range of SNR values, provided that the SNR is sufficiently large. This fact indicates that the the modified method can remove the false alarms effectively.

C. MEASUREMENT EXPERIMENT

SPU measurement results (spectrograms and detection results) are shown in Fig. 12 for three sub-bands: LTE (long term evolution)-uplink (835−845 MHz), DECT (Digital Enhanced Cordless Telecommunications) (1894.752−1903.392 MHz), and SCPC (Single Channel Per Carrier)/FDMA (Frequency Division Multiple Access) ARIB STD-T61 (450.865625−451.503125 MHz). These evaluations in Fig. 12 correspond to intuitive assessment, therefore only the results with proposed design criterion are shown. We design N_{FFT}, N_{time}, and $\mathbf{B}_{CH}$ in the three sub-bands with a target SNR=0dB and $R_t = 1/4$.

Based on the obtained spectrograms, we can confirm several characteristics of the PU SPU. In the case of LTE, the size of the minimum continuous SPU is 0.18MHz (bandwidth) and time duration of 500 μsec (time duration) as shown in Fig. 13. On the other hand, the measurement result indicates that bandwidth and time duration for one continuous SPU, (e.g., a data packet), vary dynamically.

In the case of DECT, the bandwidth and time duration for one continuous SPU are almost constant. In SCPC/FDMA, the bandwidth is constant, but the time duration varies, and it can fully occupy time domain.

The detection results in Fig. 12 capture the characteristics of the PU SPU and indicate that the SPU measurements

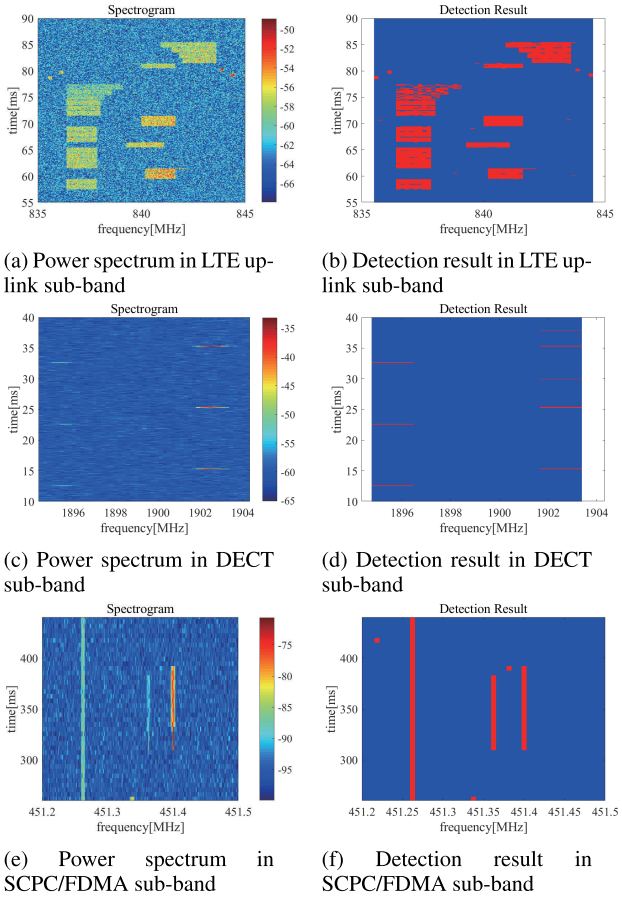

(a) Power spectrum in LTE uplink sub-band

(b) Detection result in LTE uplink sub-band

(c) Power spectrum in DECT sub-band

(d) Detection result in DECT sub-band

(e) Power spectrum in SCPC/FDMA sub-band

(f) Detection result in SCPC/FDMA sub-band

FIGURE 12. Power spectrum and detection results based on SPU measurements in LTE-uplink ((a) and (b)), DECT ((c) and (d)), and SCPC/FDMA ((e) and (f)). In the detection results, dark color and bright color correspond to $\dot{H} = H_1$ and $\dot{H} = H_0$, respectively.

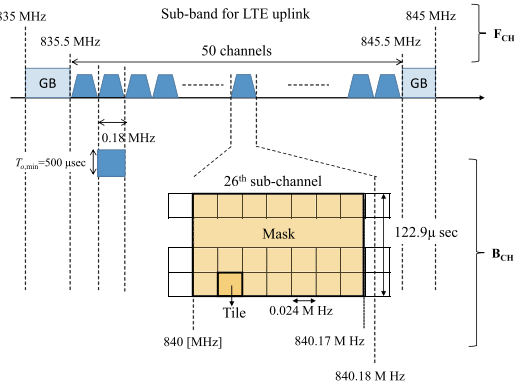

FIGURE 13. F_{CH}, B_{CH}, and mask design in sub-band LTE-uplink.

can be performed accurately with the proposed design. The design results in Figs. 13, 14, and 15 indicate two aspects. The first one is that the time duration is approximately 1/4 of $T_{O,\min}$ due to $R_t = 1/4$. The second one is that the number of frequency bins in a sub-channel is approximately seven to eight. This is because an adequate number

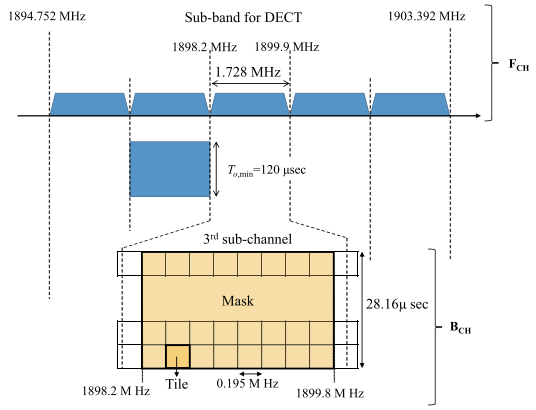

FIGURE 14. F_{CH}, B_{CH}, and mask design in sub-band DECT.

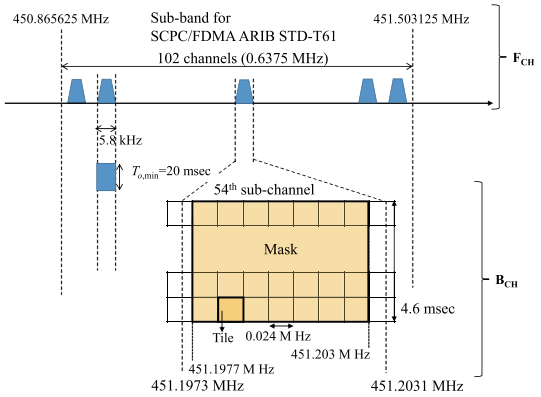

FIGURE 15. F_{CH}, B_{CH}, and mask design in sub-band SCPC/FDMA.

of bins for a sub-channel depends on the SNR as confirmed in Fig. 6 and the target SNR is set to 0 dB for the three cases.

In summary, the results of measurement experiment show that the proposed methods can achieve appropriate detection performance in the various spectrum usage scenarios. This indicates a versatility of the proposed methods.

VI. CONCLUSION

In this paper we have investigated the design of SPUD according to the SPU information. Wide-band SPU measurements cover multiple wireless systems and the characteristic of the PU SPU strongly depends on the wireless system. We have proposed a unified design framework for SPUD. In the proposed model framework, both characteristics of the PU SPU and the SPUD are modeled with appropriate model parameters. The proposed design procedure can determine adequate model parameters for SPUD based on a set of given model parameters of SPU in the target frequency band under a time resolution constraint. Numerical evaluations based on computer simulations have demonstrated the validity of the proposed design framework, and procedure. The designed SPUD can achieve high detection performance. A strict analysis of detection performance for the model pro-

cedure requires a large number of significant figures, which involves a significant computational cost. To address this problem, we employ a deflection coefficient as an approximate criterion. Numerical evaluation show that the design procedure based on the deflection coefficient can achieve a lower computational cost than that of the strict analysis while similar SPUD performance is achieved. We have investigated the trade-off between the detection performance and time resolution in the mask design. Typically, high detection performance can be achieved with a large mask size, however this leads to low time resolution. In the estimation of the SPU statistics, such as DC, a low time resolution causes critical biased errors. To address this problem, a modified DC estimation is proposed. Numerical evaluations prove that the biased errors can be removed by the modified DC estimation method under high SNR. Finally, the proposed design is also evaluated based on three empirical SPU measurement campaigns. The measurement results obtained with the proposed design indicate that the characteristics of the PU SPU can be captured accurately.

APPENDIX
EIGENVALUES AND STATISTICS OF T_{ED}

In this appendix, the eigenvalues of $E\left[\mathbf{x}_{mask,l}\mathbf{x}_{mask,l}^H\right]$ in the lth sub-channel under H_0 and H_1 are derived for (8), (9) and (14) [39]. Let $\mathbf{y}_k$ denote the kth segment of $\mathbf{x}_{mask,l}$, i.e.,

$$\mathbf{x}_{mask,l} = \begin{bmatrix} \mathbf{y}_0 \\ \mathbf{y}_1 \\ \vdots \\ \mathbf{y}_{N_{time}-1} \end{bmatrix} \tag{19}$$

and an element in $\mathbf{y}_k$, $x_{k,b}$, in the frequency region $b_l^L \le b \le b_l^H$. Let N_f denote the number of bins in the frequency region, i.e., $N_f = b_l^H - b_l^L + 1$. The FFT output for $\mathbf{y}_k$ is given by

$$\mathbf{y}_k = \mathbf{F}^{mask}\mathbf{W}\mathbf{r}_k \tag{20}$$

where $\mathbf{F}^{mask}$ is the Fourier transfer matrix for the lth sub-channel is given by

$$\mathbf{F}^{mask} = \begin{bmatrix} \alpha^0 & \alpha^{b_l^L} & \cdots & \alpha^{b_l^L(N_{FFT}-1)} \\ \alpha^0 & \alpha^{b_l^L+1} & \cdots & \alpha^{(b_l^L+1)(N_{FFT}-1)} \\ \vdots & \vdots & \ddots & \vdots \\ \alpha^0 & \alpha^{b_l^H} & \cdots & \alpha^{(b_l^H)(N_{FFT}-1)} \end{bmatrix}. \tag{21}$$

$E\left[\mathbf{x}_{mask,l}\mathbf{x}_{mask,l}^H\right]$ can be expressed in terms of $\mathbf{y}_k$ as

$$E\left[\mathbf{x}_{mask,l}\mathbf{x}_{mask,l}^H\right] = E\left[\begin{bmatrix} \mathbf{y}_0 \\ \mathbf{y}_1 \\ \vdots \\ \mathbf{y}_{N_{time}-1} \end{bmatrix}\begin{bmatrix} \mathbf{y}_0 \\ \mathbf{y}_1 \\ \vdots \\ \mathbf{y}_{N_{time}-1} \end{bmatrix}^H\right]$$

$$= \begin{bmatrix} E\left[\mathbf{y}_0\mathbf{y}_0^H\right] & E\left[\mathbf{y}_0\mathbf{y}_1^H\right] & \cdots & E\left[\mathbf{y}_0\mathbf{y}_{N_t-1}^H\right] \\ E\left[\mathbf{y}_1\mathbf{y}_0^H\right] & E\left[\mathbf{y}_1\mathbf{y}_1^H\right] & \cdots & E\left[\mathbf{y}_1\mathbf{y}_{N_t-1}^H\right] \\ \vdots & \vdots & \ddots & \vdots \\ E\left[\mathbf{y}_{N_t-1}\mathbf{y}_0^H\right] & E\left[\mathbf{y}_{N_t-1}\mathbf{y}_1^H\right] & \cdots & E\left[\mathbf{y}_{N_t-1}\mathbf{y}_{N_t-1}^H\right] \end{bmatrix} \tag{22}$$

A covariance matrix for the pth segment $\mathbf{y}_p$ and the qth segment $\mathbf{y}_q$ is then defined as

$$E\left[\mathbf{y}_p\mathbf{y}_q^H\right] = E\left[(\mathbf{F}^{mask}\mathbf{W}\mathbf{r}_p)(\mathbf{F}^{mask}\mathbf{W}\mathbf{r}_q)^H\right] = \mathbf{F}^{mask}\mathbf{W}E\left[\mathbf{r}_p\mathbf{r}_q^H\right]\mathbf{W}\mathbf{F}^{mask\,H}. \tag{23}$$

The received signal vector $\mathbf{r}_p$ is given by $\mathbf{r}_p = \mathbf{s}_p + \mathbf{z}_p$, where $\mathbf{s}_p$ and $\mathbf{z}_p$ are vectors for signal and noise components respectively. Based on the signal model $\mathbf{r}_p = \mathbf{s}_p + \mathbf{z}_p$, $E\left[\mathbf{y}_p\mathbf{y}_q^H\right]$ is given by

$$E\left[\mathbf{y}_p\mathbf{y}_q^H\right] = \mathbf{F}^{mask}\mathbf{W}E\left[\mathbf{s}_p\mathbf{s}_q^H\right]\mathbf{W}\mathbf{F}^{mask\,H} + \mathbf{F}^{mask}\mathbf{W}E\left[\mathbf{z}_p\mathbf{z}_q^H\right]\mathbf{W}\mathbf{F}^{mask\,H}. \tag{24}$$

The first and second terms in the right-hand side represent the covariance matrices of signal and noise components, respectively. Each element in $\mathbf{z}_p$ is a noise signal sample that follows an independent and identically distributed (IID) complex Gaussian distribution with zero mean and variance σ_N^2.

Regarding the second term in (24), let δ_k be a function defined by

$$\delta_k = \begin{cases} 1, & k = 0 \\ 0, & k \ne 0 \end{cases} \tag{25}$$

$\mathbf{z}_p$ is a vector with, the sampled noise components as:

$$\mathbf{z}_p = [z_{pN_{FFT}/2+1}, \ \ldots, \ z_{pN_{FFT}/2+N_{FFT}}]^t.$$

Therefore, $E\left[\mathbf{z}_p\mathbf{z}_q^H\right]$ can be expressed as a function of δ_k as

$$E\left[\mathbf{z}_p\mathbf{z}_q^H\right] = \sigma_N^2\begin{bmatrix} \delta_\Delta & \delta_{\Delta+1} & \cdots & \delta_{\Delta+N_{FFT}-1} \\ \delta_{\Delta-1} & \delta_\Delta & \cdots & \delta_{\Delta+N_{FFT}-2} \\ \vdots & \vdots & \ddots & \vdots \\ \delta_{\Delta-N_{FFT}+1} & \delta_{\Delta-N_{FFT}+2} & \cdots & \delta_\Delta \end{bmatrix}, \tag{26}$$

where $\Delta = (q-p)(1-\gamma N_{FFT})$. $\mathbf{A}_{q-p}$ is a function of $q-p$ defined by $\mathbf{A}_{q-p} = \mathbf{F}^{mask}\mathbf{W}E\left[\mathbf{z}_p\mathbf{z}_q^H\right]\mathbf{W}\mathbf{F}^{mask\,H}$. In the case of $q-p \ge 0$, $\mathbf{A}_{q-p}$ is given by

$$\mathbf{A}_{q-p} = \sigma_N^2\begin{bmatrix} \tau_{1,1} & \tau_{1,2} & \cdots & \tau_{1,N_f} \\ \tau_{2,1} & \tau_{2,2} & \cdots & \tau_{2,N_f} \\ \vdots & \vdots & \ddots & \vdots \\ \tau_{N_f,1} & \tau_{N_f,2} & \cdots & \tau_{N_f,N_f} \end{bmatrix} \tag{27}$$

where

$$\tau_{m,n} = \sum_{k=0}^{N_{FFT}-\Delta-1} w_k \alpha^{(b_l^L+m-1)k} w_{k+\Delta} \alpha^{-(b_l^L+n-1)(k+\Delta)} \quad (28)$$

In the case of $q-p<0$, $\mathbf{A}_{q-p}$ is given by $\mathbf{A}_{q-p} = \mathbf{A}_{p-q}^H$.

Regarding the first term in (24), an assumed model of the signal component in the vector $\mathbf{s}_p$ is shown as follows. The signal component at the tth time sample is denoted by $s(t)$. This signal is bandlimited to the lth sub-channel in which the center frequency and bandwidth of the sub-channel are denoted by $f_c^{(l)}$ and B^l. Specifically, $s(t)$ is defined as [44]

$$s(t) = \left(\sum_{i=-I}^{I} s_w(M_d t - i) w_s(i) \right) \exp\left(2\pi j \frac{f_c - f_c^{(l)}}{f_s} k \right), \quad (29)$$

where s_w is the signal component, which follows an IID complex Gaussian distribution with zero mean and variance σ_S^2, $w_s(i)$ is a coefficient of the bandlimiting filter, $M_u : M_d$ is the approximated smallest integer ratio of $f_s : f_c^{(l)}$. The bandlimiting filter coefficient $w_s(i)$ is set to;

$$w_s(i) = \sqrt{\frac{M_d/M_u}{\sum_{i=-L}^{L}(h(i))^2}} h(i) \quad (30)$$

where

$$h(i) = \begin{cases} \mathrm{sinc}\left(\frac{i}{M_u}\right) \frac{I_0\left(\beta\sqrt{1-(i/L)^2}\right)}{I_0(\beta)} & |i| \le L \\ 0 & otherwise, \end{cases} \quad (31)$$

$\mathrm{sinc}(x) = \sin(\pi x)/(\pi x)$, $I_0\left(\beta\sqrt{1-(l/L)^2}\right)/I_0(\beta)$ indicates Kaiser window, I_0 is modified Bessel function of the first kind and zeroth order, and β is a shape parameter for the window.

The covariance between $s(m)$ and $s(n)$, is given by

$$\begin{aligned} E\left[s(m)s^*(n)\right] &= \sigma_S^2 \left[\sum_{l=-L}^{L} w_s(i) w_s(M_d(n-m)+i) \right] \\ &\quad \cdot \exp\left(-2\pi j \frac{f_c - f_c^{(l)}}{f_s} (n-m) \right) \\ &= \sigma_S^2 \rho_{n-m}. \end{aligned} \quad (32)$$

By using ρ_{n-m}, $E\left[\mathbf{s}_p \mathbf{s}_q^H\right]$ can be expressed as

$$E\left[\mathbf{s}_p \mathbf{s}_q^H\right] = \sigma_S^2 \begin{bmatrix} \rho_\Delta & \rho_{\Delta+1} & \cdots & \rho_{\Delta+N_{FFT}-1} \\ \rho_{\Delta-1} & \rho_\Delta & \cdots & \rho_{\Delta+N_{FFT}-2} \\ \vdots & \vdots & \ddots & \vdots \\ \rho_{\Delta-N_{FFT}+1} & \rho_{\Delta-N_{FFT}+2} & \cdots & \rho_\Delta \end{bmatrix} \quad (33)$$

Now we define $\mathbf{B}_{q-p} = \mathbf{F}^{mask} \mathbf{W} E\left[\mathbf{z}_p \mathbf{z}_q^H\right] \mathbf{W} \mathbf{F}^{mask\,H}$, which is also a function of $q-p$. In the case of $q-p \ge 0$, $\mathbf{B}_{q-p}$ is given by

$$\mathbf{B}_{q-p} = \sigma_S^2 \begin{bmatrix} \kappa_{1,1} & \kappa_{1,2} & \cdots & \kappa_{1,N_f} \\ \kappa_{2,1} & \kappa_{2,2} & \cdots & \kappa_{2,N_f} \\ \vdots & \vdots & \ddots & \vdots \\ \kappa_{N_f,1} & \kappa_{N_f,2} & \cdots & \kappa_{N_f,N_f} \end{bmatrix}, \quad (34)$$

where

$$\kappa_{m,n} = \sum_{k=0}^{N_{FFT}-1} \sum_{l=0}^{N_{FFT}-1} w_k \alpha^{(I_b+m-1)k} w_l \alpha^{-(I_b+n-1)l} \rho_{D+l-k} \quad (35)$$

Again, in case of $q-p<0$, $\mathbf{B}_{q-p} = \mathbf{B}_{p-q}^H$. The expectation $E\left[\mathbf{x}_{mask,l} \mathbf{x}_{mask,l}^H\right]$ under H_0 is given by

$$E\left[\mathbf{x}_{mask,l} \mathbf{x}_{mask,l}^H | H_0\right] = \sigma_N^2 \begin{bmatrix} \mathbf{A}_0 & \mathbf{A}_1 & \cdots & \mathbf{A}_{N_{FFT}-1} \\ \mathbf{A}_1^H & \mathbf{A}_0 & \cdots & \mathbf{A}_{N_{FFT}-2} \\ \vdots & \vdots & \ddots & \vdots \\ \mathbf{A}_{N_{FFT}-1}^H & \mathbf{A}_{N_{FFT}-2}^H & \cdots & \mathbf{A}_0 \end{bmatrix} \quad (36)$$

while $E\left[\mathbf{x}_{mask,l} \mathbf{x}_{mask,l}^H\right]$ under H_1 is given by

$$\begin{aligned} E\left[\mathbf{x}_{mask,l} \mathbf{x}_{mask,l}^H | H_1\right] &= \sigma_N^2 \begin{bmatrix} \mathbf{A}_0 & \mathbf{A}_1 & \cdots & \mathbf{A}_{N_{FFT}-1} \\ \mathbf{A}_1^H & \mathbf{A}_0 & \cdots & \mathbf{A}_{N_{FFT}-2} \\ \vdots & \vdots & \ddots & \vdots \\ \mathbf{A}_{N_{FFT}-1}^H & \mathbf{A}_{N_{FFT}-2}^H & \cdots & \mathbf{A}_0 \end{bmatrix} \\ &\quad + \sigma_S^2 \begin{bmatrix} \mathbf{B}_0 & \mathbf{B}_1 & \cdots & \mathbf{B}_{N_{FFT}-1} \\ \mathbf{B}_1^H & \mathbf{B}_0 & \cdots & \mathbf{B}_{N_{FFT}-2} \\ \vdots & \vdots & \ddots & \vdots \\ \mathbf{B}_{N_{FFT}-1}^H & \mathbf{B}_{N_{FFT}-2}^H & \cdots & \mathbf{B}_0 \end{bmatrix}. \end{aligned} \quad (37)$$

Finally, the eigenvalues $\lambda_k^{(H_0)}$ and $\lambda_k^{(H_1)}$ can be obtained from (36) and (37), respectively.

Moreover, $E[T_{ED}|H_i]$ and $var[T_{ED}|H_i]$ in (14) can be obtained as

$$E[T_{ED}|H_i] = \frac{1}{N_{ave}} \sum_{k=1}^{N_{ave}} \lambda_k^{(H_i)} \quad (38)$$

$$var[T_{ED}|H_i] = \frac{1}{N_{ave}} \sum_{k=1}^{N_{ave}} \left(\lambda_k^{(H_i)}\right)^2. \quad (39)$$

REFERENCES

[1] Federal Communications Commission, "Spectrum policy task force," FCC, Washington, DC, USA, Tech. Rep. 02–135, Nov. 2002.

[2] S. Bhattarai, J.-M. J. Park, B. Gao, K. Bian, and W. Lehr, "An overview of dynamic spectrum sharing: Ongoing initiatives, challenges, and a roadmap for future research," *IEEE Trans. Cogn. Commun. Netw.*, vol. 2, no. 2, pp. 110–128, Jun. 2016.

[3] R. H. Tehrani, S. Vahid, D. Triantafyllopoulou, H. Lee, and K. Moessner, "Licensed spectrum sharing schemes for mobile operators: A survey and outlook," *IEEE Commun. Surveys Tuts.*, vol. 18, no. 4, pp. 2591–2623, 4th Quart., 2016.

[4] Q. Zhao and B. M. Sadler, "A survey of dynamic spectrum access," *IEEE Signal Process. Mag.*, vol. 24, no. 3, pp. 79–89, May 2007.
[5] I. F. Akyildiz, W.-Y. Lee, M. C. Vuran, and S. Mohanty, "NeXt generation/dynamic spectrum access/cognitive radio wireless networks: A survey," *Comput. Netw.*, vol. 50, pp. 2127–2159, Sep. 2006.
[6] M. Palolo, T. Rautio, M. Matinmikko, J. Prokkola, M. Mustonen, M. Heikkila, T. Kippola, S. Yrjola, V. Hartikainen, L. Tudose, A. Kivinen, J. Paavola, J. Okkonen, M. Makelainen, T. Hanninen, and H. Kokkinen, "Licensed shared access (LSA) trial demonstration using real LTE network," in *Proc. 9th Int. Conf. Cognit. Radio Oriented Wireless Netw. Commun. (CROWNCOM)*, Jun. 2014, pp. 498–502.
[7] M. M. Sohul, M. Yao, T. Yang, and J. H. Reed, "Spectrum access system for the citizen broadband radio service," *IEEE Commun. Mag.*, vol. 53, no. 7, pp. 18–25, Jul. 2015.
[8] M. López-Benítez, A. Al-Tahmeesschi, D. K. Patel, J. J. Lehtomäki, and K. Umebayashi, "Estimation of primary channel activity statistics in cognitive radio based on periodic spectrum sensing observations," *IEEE Trans. Wireless Commun.*, vol. 18, no. 2, pp. 983–996, Feb. 2019.
[9] N. Wang, Y. Gao, and X. Zhang, "Adaptive spectrum sensing algorithm under different primary user utilizations," *IEEE Commun. Lett.*, vol. 17, no. 9, pp. 1838–1841, Sep. 2013.
[10] T. Nguyen, B. L. Mark, and Y. Ephraim, "Spectrum sensing using a hidden bivariate Markov model," *IEEE Trans. Wireless Commun.*, vol. 12, no. 9, pp. 4582–4591, Sep. 2013.
[11] K. Umebayashi, K. Hayashi, and J. J. Lehtomäki, "Threshold-setting for spectrum sensing based on statistical information," *IEEE Commun. Lett.*, vol. 21, no. 7, pp. 1585–1588, Jul. 2017.
[12] C. Cormio and K. R. Chowdhury, "A survey on MAC protocols for cognitive radio networks," *Ad Hoc Netw.*, vol. 7, no. 7, pp. 1315–1329, Sep. 2009.
[13] K. Umebayashi, K. Kasahara, Y. Kamiya, and Y. Suzuki, "A novel spectrum sharing technique based on channel occupancy rate information," in *Proc. IEEE Global Commun. Conf. (GLOBECOM)*, Honolulu, HI, USA, Dec. 2009, pp. 1–6.
[14] M. Höyhtyä, S. Pollin, and A. Mämmelä, "Classification-based predictive channel selection for cognitive radios," in *Proc. IEEE Int. Conf. Commun. (ICC)*, May 2010, pp. 1–6.
[15] Y. Chen and H. S. Oh, "A survey of measurement-based spectrum occupancy modeling for cognitive radios," *IEEE Commun. Surveys Tuts.*, vol. 18, no. 1, pp. 848–859, 1st Quart., 2016.
[16] S. Sengottuvelan, J. Ansari, P. Mähönen, T. G. Venkatesh, and M. Petrova, "Channel selection algorithm for cognitive radio networks with heavy-tailed idle times," *IEEE Trans. Mobile Comput.*, vol. 16, no. 5, pp. 1258–1271, May 2017.
[17] K. Umebayashi, S. Tiiro, and J. J. Lehtomäki, "Development of a measurement system for spectrum awareness," in *Proc. 1st Int. Conf. 5G for Ubiquitous Connectivity*, Akaslompolo, Finland, Nov. 2014, pp. 234–239.
[18] K. Umebayashi, M. Kobayashi, and M. López-Benítez, "Efficient time domain deterministic-stochastic model of spectrum usage," *IEEE Trans. Wireless Commun.*, vol. 17, no. 3, pp. 1518–1527, Mar. 2018.
[19] D. Datla, A. M. Wyglinski, and G. J. Minden, "A spectrum surveying framework for dynamic spectrum access networks," *IEEE Trans. Veh. Technol.*, vol. 58, no. 8, pp. 4158–4168, Oct. 2009.
[20] M. López-Benítez and F. Casadevall, "Spectrum usage in cognitive radio networks: From field measurements to empirical models," *IEICE Trans. Commun.*, vol. E97-B, no. 2, pp. 242–250, Feb. 2014.
[21] M. Höyhtyä, A. Mammela, M. Eskola, M. Matinmikko, J. Kalliovaara, J. Ojaniemi, J. Suutala, R. Ekman, R. Bacchus, and D. Roberson, "Spectrum occupancy measurements: A survey and use of interference maps," *IEEE Commun. Surveys Tuts.*, vol. 18, no. 4, pp. 2386–2414, 4th Quart., 2016.
[22] F. Salahdine and H. El Ghazi, "A real time spectrum scanning technique based on compressive sensing for cognitive radio networks," in *Proc. IEEE 8th Annu. Ubiquitous Comput., Electron. Mobile Commun. Conf. (UEMCON)*, Oct. 2017, pp. 506–511.
[23] M. A. McHenry, P. A. Tenhula, D. McCloskey, D. A. Roberson, and C. S. Hood, "Chicago spectrum occupancy measurements & analysis and a long-term studies proposal," in *Proc. 1st Int. Workshop Technol. Policy Accessing Spectr.*, Boston, MA, USA, Aug. 2006, Art. no. 1.
[24] M. L. Benitez, A. Umbert, and F. Casadevall, "Evaluation of spectrum occupancy in Spain for cognitive radio applications," in *Proc. IEEE 69th Veh. Technol. Conf.*, Barcelona, Spain, Apr. 2009, pp. 1–5.
[25] V. Valenta, R. Maršálek, G. Baudoin, M. Villegas, M. Suarez, and F. Robert, "Survey on spectrum utilization in Europe: Measurements, analyses and observations," in *Proc. 5th Int. Conf. Cogn. Radio Oriented Wireless Netw. Commun. (CROWNCOM)*, Jun. 2010, pp. 1–5.
[26] R. Schiphorst and C. H. Slump, "Evaluation of spectrum occupancy in Amsterdam using mobile monitoring vehicles," in *Proc. IEEE 71st Veh. Technol. Conf.*, Taipei, Taiwan, May 2010, pp. 1–5.
[27] N. Q. B. Vo, Q. C. Le, Q. P. Le, D. T. Tran, T. Q. Nguyen, and M. T. Lam, "Vietnam spectrum occupancy measurements and analysis for cognitive radio applications," in *Proc. Int. Conf. Adv. Technol. Commun. (ATC)*, Da Nang, Vietnam, Aug. 2011, pp. 135–143.
[28] M. López-Benítez and F. Casadevall, "Empirical time-dimension model of spectrum use based on a discrete-time Markov chain with deterministic and stochastic duty cycle models," *IEEE Trans. Veh. Technol.*, vol. 60, no. 6, pp. 2519–2533, Jul. 2011.
[29] M. López-Benítez, F. Casadevall, D. López-Pérez, and A. Vasilakos, "Modeling and simulation of joint time-frequency properties of spectrum usage in cognitive radio," in *Proc. 4th Int. Conf. Cognit. Radio Adv. Spect. Manage. (CogART)*, Barcelona, Spain, Oct. 2011, pp. 1–5.
[30] S. Yin, Q. Zhang, E. Zhang, L. Yin, and S. Li, "Statistical modeling for spectrum usage characterizing wireless fading channels and mobile service dynamics," *IEEE Trans. Veh. Technol.*, vol. 62, no. 8, pp. 3800–3812, Oct. 2013.
[31] M. López-Benítez and F. Casadevall, "Space-dimension models of spectrum usage for cognitive radio networks," *IEEE Trans. Veh. Technol.*, vol. 66, no. 1, pp. 306–320, Jan. 2017.
[32] A. Gupta, S. Agarwal, and S. De, "A new spectrum occupancy model for 802.11 WLAN traffic," *IEEE Commun. Lett.*, vol. 20, no. 12, pp. 2550–2553, Dec. 2016.
[33] M. O. Al Kalaa, M. Ghanem, H. H. Refai, and S. J. Seidman, "PESA: Probabilistic efficient storage algorithm for time-domain spectrum measurements," *IEEE Trans. Instrum. Meas.*, vol. 68, no. 2, pp. 325–333, Feb. 2019.
[34] K. Umebayashi, R. Takagi, N. Ioroi, Y. Suzuki, and J. J. Lehtomäki, "Duty cycle and noise floor estimation with Welch FFT for spectrum usage measurements," in *Proc. Cognit. Radio Oriented Wireless Netw. Commun. (CROWNCOM)*, Oulu, Finland, Jun. 2014, pp. 73–78.
[35] H. Iwata, K. Umebayashi, S. Tiiro, J. J. Lehtomäki, M. López-Benítez, and Y. Suzuki, "Welch FFT segment size selection method for spectrum awareness system," *IEICE Trans. Commun.*, vol. E99-B, no. 8, pp. 1813–1823, 2016.
[36] J. J. Lehtomaki, J. Vartiainen, M. Juntti, and H. Saarnisaari, "CFAR outlier detection with forward methods," *IEEE Trans. Signal Process.*, vol. 55, no. 9, pp. 4702–4706, Sep. 2007.
[37] P. D. Welch, "The use of fast Fourier transform for the estimation of power spectra: A method based on time averaging over short, modified periodograms," *IEEE Trans. Audio Electroacoust.*, vol. 15, no. 2, pp. 70–73, Jun. 1967.
[38] K. Umebayashi, K. Moriwaki, R. Mizuchi, H. Iwata, S. Tiiro, J. Lehtomäki, M. López-Benítez, and Y. Suzuki, "Simple primary user signal area estimation for spectrum measurement," *IEICE Trans. Commun.*, vol. E99-B, no. 2, pp. 523–532, Feb. 2016.
[39] W. Sichun, F. Patenaude, and R. J. Inkol, "Computation of the normalized detection threshold for the FFT filter bank-based summation CFAR detector," *J. Comput.*, vol. 2, no. 6, pp. 35–48, Aug. 2007.
[40] J. J. Lehtomaki, R. Vuohtoniemi, and K. Umebayashi, "On the Measurement of Duty Cycle and Channel Occupancy Rate," *IEEE J. Sel. Areas Commun.*, vol. 31, no. 11, pp. 2555–2565, Nov. 2013.
[41] S. M. Kay, *Fundamentals of Statistical Signal Processing, Volume II: Detection Theory*. Upper Saddle River, NJ, USA: Prentice-Hall, 1998.
[42] B. Shen, S. Ullah, and K. Kwak, "Deflection coefficient maximization criterion based optimal cooperative spectrum sensing," *Int. J. Electron. Commun.*, vol. 64, no. 9, pp. 819–827, Sep. 2009.
[43] K. Umebayashi, H. Tsuchiya, and Y. Suzuki, "Analysis of optimal weighted cooperative spectrum sensing with multiple antenna elements," *IEICE Trans. Commun.*, vol. E95-B, no. 10, pp. 3261–3269, Oct. 2009.
[44] A. Oppenheim, *Discrete-Time Signal Processing*. London, U.K.: Pearson, 2013.

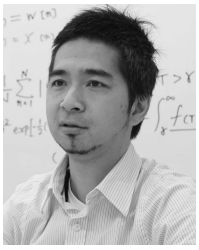

KENTA UMEBAYASHI (S'00–M'04) received the B.E., M.E., and Ph.D. degrees from Yokohama National University, Japan, in 1999, 2001, and 2004, respectively, and the L.L.B. degree from Ritsumeikan University, Japan, in 1996. From 2004 to 2006, he was a Research Scientist with the Centre for Wireless Communications, University of Oulu, Finland. He was a Principal Investigator of four grants-in-aid for scientific research projects and three strategic information and communications research and development promotion program projects. He is currently an Associate Professor with the Tokyo University of Agriculture and Technology, Japan. His research interests include the areas of signal detection and estimation theories for wireless communication, signal processing for multiple antenna systems, cognitive radio networks, and terahertz band wireless communications. He received the Best Paper Award at the 2012 IEEE WCNC and the Best Paper Award at the 2015 IEEE WCNC Workshop from IWSS.

YOSHITAKA TAMAKI received the B.E. and M.E. degrees from the Tokyo University of Agriculture and Technology, Tokyo, Japan, in 2016 and 2018, respectively. He has been with TAIKI-SHA Ltd., since 2019. His research interests include cognitive radio and wireless communication systems.

MIGUEL LÓPEZ-BENÍTEZ (S'08–M'12–SM'17) received the B.Sc. and M.Sc. degrees (Hons.) in telecommunication engineering from Miguel Hernández University, Elche, Spain, in 2003 and 2006, respectively, and the Ph.D. degree *(summa cum laude)* in telecommunication engineering from the Technical University of Catalonia, Barcelona, Spain, in 2011.

He was a Research Fellow with the Centre for Communication Systems Research, University of Surrey, U.K., from 2011 to 2013. In 2013, he became a Lecturer (Assistant Professor) at the Department of Electrical Engineering and Electronics, University of Liverpool, U.K., and was promoted to Senior Lecturer (Associate Professor), in 2018, which is his current position. Since 2018, he has been an Affiliate Senior Research Associate with the ARIES Research Centre, Antonio de Nebrija University, Madrid, Spain. His research interests include the fields of wireless communications and networking, with special emphasis on mobile communications and dynamic spectrum access in cognitive radio systems. He has been a member of the Organising Committee for the IEEE WCNC International Workshop on Smart Spectrum (IWSS 2015–2019) and the Track Co-Chair of the 89th IEEE Vehicular Technology Conference (VTC 2019-Spring). He has been the Principal Investigator or a Co-Investigator of research projects funded by the EPSRC, the British Council, and the Royal Society and has been involved in the European-funded projects: AROMA, NEWCOM++, FARAMIR, QoSMOS, and CoRaSat. He is also an Associate Editor of the IEEE Access, *IET Communications*, and *Wireless Communications and Mobile Computing*. Please visit http://www.lopezbenitez.es for more details.

JANNE J. LEHTOMÄKI (S'03–M'06) received the Ph.D. degree from the University of Oulu, Finland, in 2005, where he is currently an Adjunct Professor with the Centre for Wireless Communications. In 2013, he spent a semester with Georgia Tech, Atlanta, GA, USA, as a Visiting Scholar. He is currently focusing on spectrum measurements and terahertz band wireless communication. He is also an Editorial Board Member of *Physical Communication*. He was a recipient of the Best Paper Award at the IEEE WCNC 2012 for his coauthored paper. He was the General Co-Chair of the IEEE WCNC 2017 International Workshop on Smart Spectrum, the TPC Co-Chair of the IEEE WCNC 2015 and the 2016 International Workshop on Smart Spectrum, and the Publicity/Publications Co-Chair of the ACM NANOCOM 2015, 2016, and 2017. He has served as a Guest Associate Editor for the *IEICE Transactions on Communications* Special Section, in 2014 and 2017, and as a Managing Guest Editor for the *Nano Communication Networks* Special Issue, in 2016.